

Crystal and magnetic structure of new superconductor $\text{CeNi}_{0.8}\text{Bi}_2$

K. Kodama,^{1,2} S. Wakimoto,^{1,2} N. Igawa,¹ S. Shamoto,^{1,2} H. Mizoguchi,³ and H. Hosono^{3,4}

¹Quantum Beam Directorate, Japan Atomic Energy Agency, Tokai, Ibaraki 319-1195, Japan

²JST, Transformative Research-Project on Iron Pnictides (TRIP), Tokyo 102-0075, Japan

³Frontier Research Center, Tokyo Institute of Technology, Nagatsuta, Yokohama 226-8503, Japan

⁴Materials and Structures Laboratory, Tokyo Institute of Technology, Nagatsuta, Yokohama 226-8503, Japan

(Dated: June 2, 2019)

We have performed powder neutron diffraction on new superconductor, $\text{CeNi}_{0.8}\text{Bi}_2$ with superconducting transition temperature $T_c \sim 4.2$ K. The structural parameters of this compound at room temperature are determined by Rietveld analysis. Below about 5 K, the clear magnetic Bragg peaks with propagation vector $q=(0\ 0\ 0)$ are observed. The observed intensities of magnetic Bragg peaks can be explained by the magnetic structure that the two Ce moments in the unit cell are antiparallel along c -axis. The magnetic Bragg peaks are observed in superconducting state, indicating the coexistence of the antiferromagnetic ordering and the superconductivity in this compound. The intensity of magnetic Bragg peak monotonously increases with decreasing temperature below T_N and does not exhibit apparent anomaly at T_c , obviously different from the cases of the heavy fermion superconductors in which the magnetic ordering and the superconductivity coexist, for example, Cd-doped CeCoIn_5 . These results suggest that the $4f$ electron of Ce atom does not couple with the superconducting carrier and the magnetic ordering almost independent of the superconductivity in $\text{CeNi}_{0.8}\text{Bi}_2$.

PACS numbers: 74.25.Ha, 75.25.-j, 61.05.F-, 61.66.Fn

I. INTRODUCTION

Iron-based superconductor was firstly discovered in LaFeAsO system with so-called ZrCuSiAs -type structure whose superconductivity is induced by partial substitution of fluorine for oxygen.¹ After this discovery, the development of new similar materials with Fe layer in which the superconductivity is considered to appear, have been performed, resulting in the discoveries of other iron-based superconductors, such as so-called 122 system,² $\text{FeSe}_{1-x}\text{Te}_x$,³ LiFeAs ,⁴ and so on. On the other hand, new superconductors with ZrCuSiAs -type structure which consist of other elements than Fe are also explored, for example, $\text{La}_{1-x}\text{Sr}_x\text{NiAsO}$.⁵ Recently, Mizoguchi and his collaborators have discovered the superconductivity in $\text{CeNi}_{0.8}\text{Bi}_2$ with superconducting transition temperature $T_c \sim 4.2$ K.⁶

Series compounds CeMBi_2 and CeMSb_2 have ZrCuSiAs -type structure with space group of $P4/nmm$ corresponding with so-called 1111 system, where M is a transition metal element such as Mn, Fe, Ni, Cu, Ag, and so on.⁷ For CeMBi_2 , Bi1, M, Ce and Bi2 sites correspond to As, Fe, rare earth element and O sites, respectively. "Parent" compound of $\text{CeNi}_{0.8}\text{Bi}_2$, CeNiBi_2 is a moderate heavy fermion antiferromagnet; magnetic ordering appears at about 5 K and the electronic specific heat coefficient γ is relatively large (470 mJ/K² mol).⁸ This parent compound does not exhibit a superconductivity although the electric conductivity is metallic at lowest temperature.^{8,9}

The superconductivity is induced by the deficiency of Ni atom,⁶ as the superconductivity in the iron-based superconductor of so-called 1111 system is induced by oxygen-deficiency.¹⁰ The resistivity and superconducting

shielding signal in the magnetic field show the superconducting transition at about 4.2 K. At about 5 K, the specific heat C exhibits the jump of ~ 4 J/K mol. This jump may be attributed to the magnetic ordering of Ce $4f$ moment because the entropy estimated by the integration of C/T below 5 K corresponds with $R\ln 2$ which is expected from the two-fold degenerated ground state of Ce $4f$ electron. The clear jump of the specific heat is not observed at around T_c because the jump caused by the superconducting transition is much smaller than the jump caused by the magnetic ordering, suggesting that the charge carrier which causes the superconductivity does not couple with the Ce $4f$ electron and the mass is not enhanced.⁶

If the Ce $4f$ electron couples with the superconducting carrier in the present compound, the magnetic fluctuation of $4f$ electron can induce the unconventional superconducting order parameter. In such case, temperature dependence of the magnetic Bragg peak should have some anomaly at T_c . Then we have performed powder neutron diffraction measurements on $\text{CeNi}_{0.8}\text{Bi}_2$ in order to investigate an existence of the coupling between Ce $4f$ electron and superconducting carrier. First, we present the structural parameters determined by Rietveld analysis in §III-A. The electronic state of this compound discussed in the previous letter⁶ is based on the present result. In §III-B, we report the magnetic structure and the temperature dependence of the ordered moment of Ce- $4f$ moment. Our results suggest that the Ce- $4f$ electron does not contribute to the superconductivity in this compound, consistent with the suggestion in ref. 6.

II. EXPERIMENTS

For the compound of CeNi_xBi_2 , we found through a series of synthesis experiments that samples synthesized by conventional solid state reaction have a constant Ni-deficiency of $x=0.8$.⁶ Powder sample of $\text{CeNi}_{0.8}\text{Bi}_2$ for present neutron measurements was prepared by following method. Ce, Ni and Bi powder with nominal composition of $\text{CeNi}_{0.8}\text{Bi}_2$ was used as starting materials. The mixed powder was evacuated in silica tube and heated at 500 °C for 10 hours and 750 °C 20 hours. The obtained powder was reground and pressed into pellets, and it was heated 800 °C for 10 hours in the evacuated silica tube. Inductively coupled plasma (ICP) spectroscopy was used to confirm the chemical composition, $\text{CeNi}_{0.8}\text{Bi}_2$, which was consistent with the nominal composition. The sample appears stable thermally in a dry box or an evacuated glass tube, but decomposed in a hour when they are exposed to an ambient atmosphere. This decomposition would be induced by the reaction of unusual valence state of Bi ions in the material with water vapor in the atmosphere. Thus, we paid attention so as to avoid the decomposition or degradation of the sample. The sample of about 14.3 g was used in neutron diffraction measurements.

The powder neutron diffraction pattern for the analysis on crystal structure was collected by using the high-resolution powder diffractometer HRPD installed in the reactor JRR-3 of JAEA. The neutron wave length was 1.8234 Å and the collimation was open (effective value of 35'-40'-S-6' (S denotes sample)). The pattern was collected at room temperature. The powder sample was set in vanadium holder enclosed in Al cans filled with He gas in order to avoid the decomposition in the atmosphere. Diffraction data for the analysis on magnetic structure were collected using the triple axes spectrometer TAS-2 in the reactor JRR-3 of JAEA. Used neutron wave length was 2.3590 Å and the collimation was 14'-40'-S-40'-80'. The powder sample was set in vanadium holder enclosed in Al can filled with He gas. The sample was mounted in a closed-cycle refrigerator.

III. RESULTS AND DISCUSSIONS

A. Analysis of crystal structure

Figure 1 shows the neutron powder diffraction patterns of $\text{CeNi}_{0.8}\text{Bi}_2$ obtained at HRPD. The observed data are shown by crosses. Structural analyses on neutron powder diffraction data are performed by using the program RIETAN2000.¹¹ The space group of $P4/nmm$ is used because we know that the series compounds of CeMBi_2 and CeMSb_2 have same structure as shown in §I. The diffraction pattern is analyzed including NiBi_3 , NiBi and Ni as impurities. Because a small peak which can not be assigned by above impurities is observed at $2\theta \sim 61.2^\circ$, the intensity data in the 2θ -range of 60.9-61.5 ° are excluded

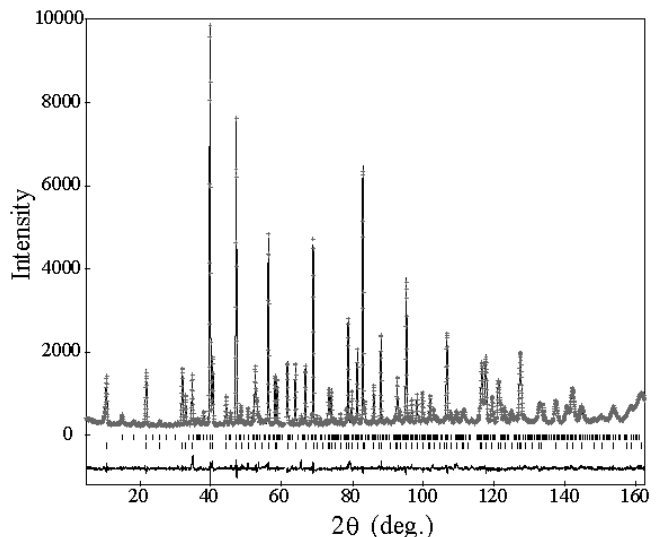


FIG. 1: Observed (crosses) and calculated (solid lines) neutron powder diffraction pattern of $\text{CeNi}_{0.8}\text{Bi}_2$. Observed pattern is collected by using HRPD at room temperature. Vertical bars show the calculated position of Bragg reflections including the impurities. The solid line at the bottom of the figure is the difference between observed and calculated intensities

TABLE I: Atomic positions of $\text{CeNi}_{0.8}\text{Bi}_2$ (space group $P4/nmm$) determined by Rietveld analysis of neutron powder diffraction data at room temperature. Obtained lattice parameters are $a=4.5439(1)$ and $c=9.6414(2)$ Å. The R -factor, R_{wp} , is 6.04 %,

Atom	Site	Occ.	x	y	z	B (Å ²)
Ce	2c	1	1/4	1/4	0.2691(3)	0.83(4)
Ni	2b	0.8	3/4	1/4	1/2	1.83(4)
Bi1	2c	1	1/4	1/4	0.6384(2)	0.92(3)
Bi2	2a	1	3/4	1/4	0	0.66(4)

in the analysis. The occupation factor of Ni is fixed at 0.8 which is determined by ICP spectroscopy. The obtained structural parameters of $\text{CeNi}_{0.8}\text{Bi}_2$ are shown in Table I. The errors of the parameters shown in the table are mathematical standard deviations obtained by the analysis. The diffraction patterns calculated by using refined parameters are shown in Fig. 1 by solid lines. The calculated lines can reproduce the observed data. Mass fractions of the impurities are 9.1 % for NiBi_3 , 1.4 % for NiBi and 0.8 % for Ni, respectively. Larger thermal parameter of Ni relative to other sites may be due to the impurities.

B. Magnetic structure and T dependence of ordered Ce moment

Results of 2θ scan at 11.2 K and 2.9 K, obtained at TAS-2 are shown in Fig. 2(a) by gray and black lines, respectively. At 2.9 K the clear Bragg peak appears

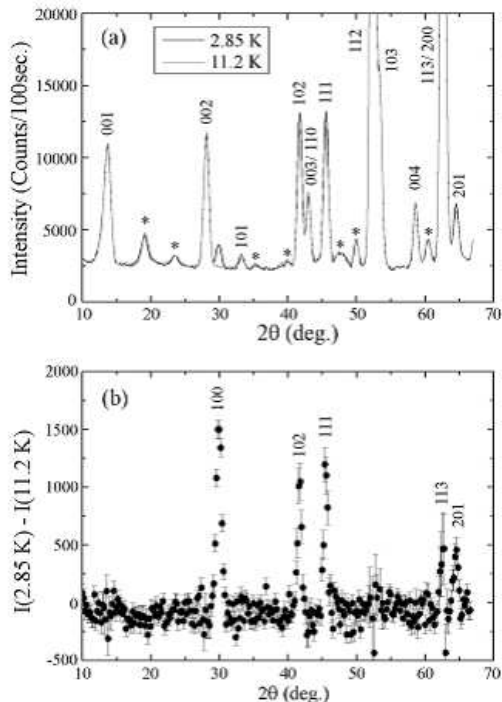


FIG. 2: (a) Neutron powder diffraction patterns of $\text{CeNi}_{0.8}\text{Bi}_2$ obtained at 11.2 K (gray line) and 2.9 K (black line). The data are collected by using TAS-2. Miller indices are shown for nuclear Bragg peaks. The peaks marked by asterisks are contributed from impurities, for example, NiBi_3 . (b) Magnetic Bragg intensity obtained by subtracting the intensity at 11.2 K from the intensity at 2.9 K.

at right side of 002 reflection, corresponding to 100 reflection. The intensities of 102 and 111 reflections are slightly enhanced at 2.9 K. These results show the existence of magnetic ordering at lower temperature and the coexistence of magnetic ordering and the superconductivity. In Fig. 2(b), the intensity obtained by subtracting the intensity at 11.2 K from the intensity at 2.9 K. Clear magnetic Bragg peaks are observed at lower temperature at the reciprocal lattice points corresponding to 100, 102, 111 and 201. The data are scattered around $2\theta \sim 53^\circ$ and 63° , due to large nuclear Bragg intensities of 112/103 and 113/200 reflections whose intensities are about 70000 and 50000 counts at their peak positions, respectively. Magnetic 113 reflection does not have clear peak profile due to the large experimental error mentioned above although it should have almost same intensity with magnetic 201 reflection in the magnetic structure presented below.

Based on these results, we can consider the magnetic structure at low temperature. For $10l$ reflection, the clear

magnetic Bragg peaks are observed at $l = 2n$ and they are nearly absent at $l = 2n + 1$, indicating that the magnetic moments of two Ce atoms in unit cell at $(1/4 \ 1/4 \ 0.2691)$ and $(3/4 \ 3/4 \ 0.7309)$ are antiparallel. This intensity modulation of magnetic $10l$ reflections against l also shows that Ni-moments are almost independent of observed magnetic Bragg peaks even if the Ni atoms have magnetic moments. The scattering intensity from the Ni-moments should not depend on l because two Ni atoms are located on flat layer at $z=1/2$. The clear peaks are not observed at $00l$ position in Fig. 2(b). If the Ce-moments are perpendicular to c -axis, magnetic $00l$ reflections with $l = 2n + 1$ must have large intensities. Especially, the intensity of 001 reflection is expected to be about four times as large as the intensity of 100 reflection. The absence of magnetic $00l$ reflections indicates that the two Ce moments are oriented along c -axis. It is consistent with the anisotropy of the magnetic susceptibility indicating that the antiferromagnetic easy-axis is c -axis.⁸ Then we can get the magnetic structure shown in Fig. 3. In the figure, Ce atom at $(1/4 \ 1/4 \ 0.2691)$ is

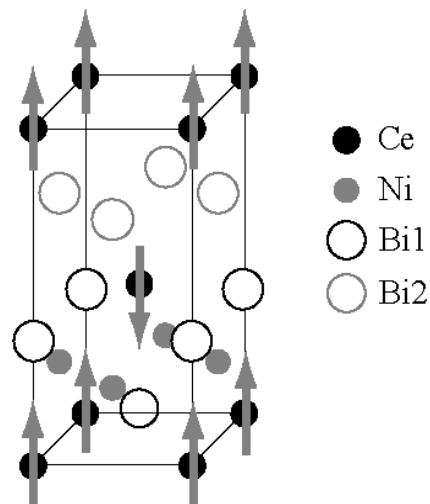


FIG. 3: Crystal and magnetic structure of $\text{CeNi}_{0.8}\text{Bi}_2$. Ce atom at $(1/4 \ 1/4 \ 0.2691)$ is origin. Gray arrows show the magnetic moments of Ce atoms.

located at the origin.

The integrated intensities, I_{obs} , of observed nuclear and magnetic Bragg reflections are shown in Table II. The former intensities are estimated by using the diffraction data at 11.2 K and the latter ones are estimated by using the data obtained by subtracting the intensity at 11.2 K from the intensity at 2.9 K, shown in Fig. 2(b). The intensities of nuclear Bragg reflections, I_{cal} , calculated by using the structural parameters shown in table I are also shown in right side of I_{obs} in the table. The calculated intensities almost correspond with the observed intensities. In order to estimate the ordered moment of Ce sites at 2.9 K, the intensities of magnetic reflections obtained from the magnetic structure shown in Fig. 3 are fitted to the observed intensities by using least-squares fitting

TABLE II: Observed and calculated intensities of nuclear (left side) and magnetic (right side) Bragg peaks. Calculated intensities are obtained by using the structural parameters shown in table I. In the calculation of magnetic Bragg intensity, we use the amplitude of Ce moment of $1.43 \mu_B$ and isotropic magnetic form factor of Ce^{3+12} .

nuclear Bragg at 11.2 K			magnetic Bragg at 2.9 K		
<i>hkl</i>	I_{obs}	I_{cal}	<i>hkl</i>	I_{obs}	I_{cal}
0 0 1	8354(428)	10316	1 0 0	1579(128)	1594
0 0 2	8354(152)	8607			
1 0 1	759(93)	652			
1 0 2	7148(301)	7734	1 0 2	827(141)	715
003/110	3643(200)	3843			
1 1 1	7490(304)	5111	1 1 1	905(149)	1008
1 1 2	51380(951)	52171			
1 0 3	10002(325)	7569			
0 0 4	3626(108)	3520			
113/200	38757(1001)	40004			
2 0 1	2842(231)	2418	2 0 1	363(123)	200

program. The estimated value of the ordered moment is $1.43(5) \mu_B$. The calculated intensities of magnetic Bragg reflections are shown in the right side of the table. The calculated intensities agree with the observed intensities, indicating that present magnetic structure and the obtained ordered moment are reasonable. Although 113 reflection should have the intensity of ~ 200 in the calculation, the observed intensities can not be estimated due to the experimental error, as mentioned above.

The inset of Fig. 4(a) is the T -dependence of the peak profile of 100 reflection. As shown in the inset, 100 reflection appears below 5.45 K and the peak gradually develops with decreasing T . Figures 4(a) and 4(b) show the T -dependences of the integrated intensities of 100 and 102 reflections, respectively. The intensity of 102 reflection has large error bar in this scale because this reflection includes the nuclear scattering. The intensities of both reflections increase with decreasing T below about 5 K, consistent with the temperature at which the jump of the specific heat is observed.⁶ As shown in the main panel of Fig. 4(a), the temperature development of the magnetic Bragg intensity is monotonous down to 2.9 K and any anomaly is not observed at the superconducting transition temperature, 4.2 K. It is quite different from the behaviors observed in heavy fermion superconductors in which the magnetic ordering and the superconductivity coexist. For example, Cd-doped $CeCoIn_5$, $CeCo(In_{1-x}Cd_x)_5$ with $x=0.1$ and 0.075 , exhibit the antiferromagnetic orderings of Ce moment at $T_N \sim 3.0$ K and 2.5 K, respectively. Superconductivities appear below ~ 1.2 K and 1.7 K, and the antiferromagnetic ordering and the superconductivity coexist below these temperatures.¹³ In these compounds, the magnetic Bragg peaks appear below T_N and their intensities increase with decreasing T . However, the developments of the magnetic Bragg intensities are suppressed and they become almost flat to the tem-

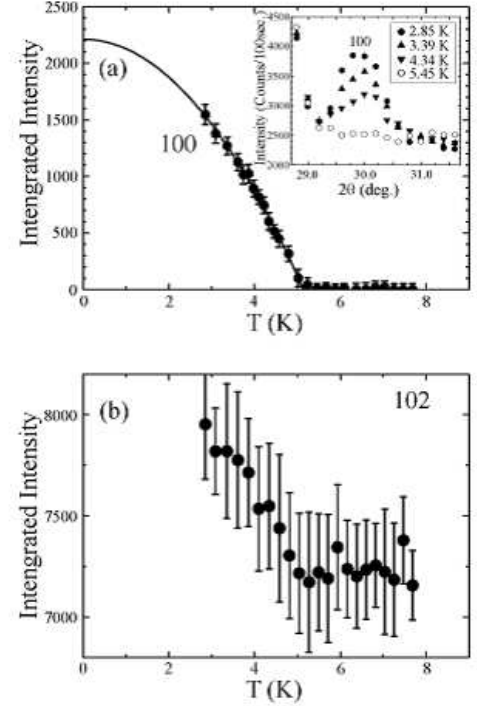


FIG. 4: Temperature dependences of the integrated intensities of 100 (a), and 102 (b) reflections, respectively. The solid line shows the fitting the data below 5 K to the function that the intensity is proportional to $1 - (T/T_N)^2$ and the extrapolation of the fitting function to zero kelvin. In the inset : temperature dependence of the peak profile of 100 reflection.

perature below T_c .^{14,15} The present T -dependence of the magnetic Bragg intensity suggests that the Ce $4f$ electron is almost independent of the superconductivity and this compound is not a heavy fermion superconductor.

The solid line in Fig. 4(a) shows the fitting the data below 5.0 K to the function that the intensity is proportional to $1 - (T/T_N)^2$ and the extrapolation of the fitting function to zero kelvin. The amplitude of the moment at zero kelvin obtained by the fitting is $1.71 \mu_B$. In the tetragonal symmetry, energy levels of Ce $4f^1$ state split into three doublets by the crystalline electric field. In the case of $CeAgSb_2$ which also has $ZrCuSiAs$ -type structure, the ground state is the Γ_6 state with $J_z = \pm 1/2$, revealed by the measurement of crystalline electric-field excitation. The amplitude of the antiferromagnetic ordered moment is in good agreement with $gJ\mu_B J_z \sim 0.43 \mu_B$.¹⁶ On the other hand, the ordered moment in this compound is much larger than the moment of $CeAgSb_2$, indicating that the ground state of this compound is not Γ_6 state and consists of the linear combination of $J_z = \pm 3/2$ and $J_z = \pm 5/2$ states. Such difference of the amplitude of the ordered moment and/or the ground state is caused by the differences of the structural parameters and constituent elements.

IV. SUMMARY

We have performed the neutron powder diffraction measurements on a new superconductor, $\text{CeNi}_{0.8}\text{Bi}_2$ with $T_c \sim 4.2$ K. The structural parameters at room temperature are determined by the Rietveld methods. The clear magnetic Bragg peaks are observed at $q=(0\ 0\ 0)$ below about 5 K. In the magnetic ordering phase, the two Ce moments in the unit cell are antiparallel along c -axis and Ni-moments do not contribute to the magnetic Bragg reflections. Below T_c , the superconductivity and antiferromagnetic ordering coexist. The magnetic Bragg intensity monotonously increases with decreasing T below about 5 K, and does not exhibit apparent anomaly at

$T_c \sim 4.2$ K, suggesting that the $4f$ electron of Ce atom is almost independent of the superconductivity. The saturated ordered moment is about $1.7\ \mu_B$.

Acknowledgments

The authors would like to thank K. Kaneko for his fruitful discussions. This work was supported by the Funding Program for World-Leading Innovative R&D on Science and Technology (FIRST), Japan, and also supported by a Grant-in-Aid for Specially Promoted Research 17001001 from the Ministry of Education, Culture, Sports, Science and Technology, Japan.

-
- ¹ Y. Kamihara, T. Watanabe, M. Hirano, and H. Hosono, J. Am. Chem. Soc. **130**, 3296 (2008).
 - ² M. Rotter, M. Tegel, D. Johrendt, Phys. Rev. Lett. **101**, 107006 (2008).
 - ³ F.-C. Hsu, J.-Y. Luo, K.-W. Yeh, T.-K. Chen, T.-W. Huang, P. M. Wu, Y.-C. Lee, Y.-L. Huang, Y.-Y. Chu, D.-C. Yan, and M.-K. Wu, Natl. Acad. Sci. U.S.A. **105**, 14262 (2008).
 - ⁴ X. C. Wang, Q. Q. Liu, Y. X. Lv, W. B. Gao, L. X. Yang, R. C. Yu, F. Y. Li, and C. Q. Jin, Solid State Commun. **148**, 538 (2008).
 - ⁵ L. Fang, H. Yang, P. Cheng, X. Zhu, G. Mu and H.-H. Wen, Phys. Rev. B **78**, 104528 (2008).
 - ⁶ H. Mizoguchi, S. Matsuishi, M. Hirano, M. Tachibana, E. Takayama-Muromachi, H. Kawaji, and H. Hosono, Phys. Rev. Lett. in press, arXiv:1011.6147.
 - ⁷ H. Flandorfer, O. Sologub, C. Godart, K. Hiebl, A. Leithe-Jasper, P. Rogl, and H. Noël, Solid State Commun. **97**, 561 (1996).
 - ⁸ A. Thamizhavel, A. Galatanu, E. Yamamoto, T. Okubo, M. Yamada, K. Tabata, T. C. Kobayashi, N. Nakamura, K. Sugiyama, K. Kindo, T. Takeuchi, R. Settai, and Y. Ōnuki, J. Phys. Soc. Jpn. **72**, 2632 (2003).
 - ⁹ M. H. Jung, A. H. Lacerda, and T. Takabakake, Phys. Rev. B **65**, 132405 (2002).
 - ¹⁰ H. Kito, H. Eisaki, and A. Iyo, J. Phys. Soc. Jpn. **77**, 063707 (2008).
 - ¹¹ F. Izumi and T. Ikeda, Mater. Sci. Forum, **321-324**, 198 (2000).
 - ¹² P. J. Brown, *International Tables for Crystallography*, edited by A. J. C. Wilson (Kluwer Academic, Dordrecht, 1992), Vol. C, Chap. 4.
 - ¹³ L. D. Pham, Tuson Park, S. Maquilon, J. D. Thompson, and Z. Fisk, Phys. Rev. Lett. **97**, 056404 (2006).
 - ¹⁴ M. Nicklas, O. Stockert, Tuson Park, K. Habicht, K. Kiefer, L. D. Pham, J. D. Thompson, Z. Fisk, and F. Steglich, Phys. Rev. B **76**, 052401 (2007).
 - ¹⁵ Sunil Nair, O. Stockert, U. Witte, M. Nicklas, R. Schedler, K. Kiefer, J. D. Thompson, A. D. Bianchi, Z. Fisk, S. Wirth, and F. Steglich, Proc. Nat. Acad. Sci. U.S.A. **107**, 9537 (2010).
 - ¹⁶ S. Araki, N. Metoki, A. Galatanu, E. Yamamoto, A. Thamizhavel, and Y. Ōnuki, Phys. Rev. B **68**, 024408 (2003).